DOI: 10.24425/amm.2019.129486

S. BOCZKAL*[#], M. KARAŚ*, P. KORCZAK*, D. KAPINOS*, P. KOPROWSKI*,
W. SZYMAŃSKI*, S. WROŃSKI**

THE INFLUENCE OF PLASTIC FORMING PROCESSES ON THE DISSOLUTION RATE OF BIOCOMPATIBLE Mg ALLOYS

The effect of plastic deformation process on the dissolution rate of biocompatible Mg alloys was investigated. Two biocompatible MgLi1Ca0,2Zn1 and MgLi1Ca1Zn1 alloys were selected for the study. The alloys were deformed on a 100T press at a temperature of 350°C by conventional extrusion and by the equal channel angular extrusion process (ECAE). The grain size analysis showed a high degree of the grain refinement from approximately 110 mm in the initial state to 2.8 mm after the 3rd pass of the ECAE process. Compared to as-cast state, the degree of strengthening has increased after plastic forming. The results of biodegradation tests have shown a significant increase in corrosion rate after both conventional extrusion and ECAE, although after subsequent ECAE passes, this rate was observed to slightly decrease in the MgLi1Ca1Zn1 alloy. Based on the results of macro- and microstructure examinations, the corrosion progress in samples after the extrusion process was described.

Keywords: MgLiCaZn alloys, biomaterials, structure and properties, immersion test

Introduction

Metal implants developed by scientists for current medical applications must show a number of necessary properties, which include strength, resistance to cyclic fatigue and biocompatibility. Biomaterials such as steel, titanium or Co-Cr alloys are characterized by the rigidity and strength far beyond the properties of natural bone. Additionally, these materials introduced into the body generate the risk of weakening the immunity system as a result of corrosion processes and the release of toxic metal ions [1]. In terms of physicochemical properties, implants made of magnesium alloys are an interesting alternative to non-resorbable metallic biomaterials. Magnesium and its alloys are light materials whose mechanical properties and modulus of elasticity are similar to natural bone, and – more important even – they are completely biodegradable in living organisms. Magnesium is, moreover, an essential component of human metabolism and is the fourth most numerous cation in the human body [2]. However, the task of developing a biomaterial for implants completely resorbable by the human body faces many problems that require solutions in the field of materials engineering and biomedicine. One of the issues that need to be solved is the effect of individual elements constituting magnesium alloys on properties, and in particular on the rate of corrosion in physiological fluids, as well as biocompatibility in vitro and in vivo [3]. Ca, Zn, Li and small amounts of RE elements are considered the most biocompatible additives introduced into magnesium. The composition and amount of alloy additives contribute to the change of strength properties and corrosion. Calcium is the most important bone mineral. Present in an amount of over 1%, calcium in magnesium alloys improves corrosion resistance and has low mechanical properties. In magnesium alloys, Ca forms CaMg2 phases [4-6]. The addition of Ca to magnesium alloys reduces hydrogen evolution and thus increases the corrosion resistance [1]. Zinc increases mechanical properties, especially during heat treatment, and reduces the corrosion rate of the alloy compared to pure Mg. In the alloy it forms with Mg the MgZn2 phase [7,8].

Mg-Li alloys are characterized by good plasticity and formability combined with high strength and stiffness. The addition of Li to magnesium reduces the c/a ratio of the crystal lattice parameter, resulting in easier slipping of systems in the prismatic planes [9]. The higher content of lithium in magnesium (8.5% Li) contributes to an increase in the biodegradation speed. The source of this increase in Mg-Li alloys is to be sought in an increased proportional fraction of the β phase of a regular lattice [10]. In addition to strength properties and corrosion rates, an important feature of implants based on magnesium alloys is their biocompatibility tested in an immersion test. This test is carried out in a simulated body fluid (SBF), buffered saline (PBS) and minimum essential medium (αMEM). The pH level control and observations carried out in time allow qualifying the material as biocompatible. Pure magnesium is reconstituted in a pH 7.4-7.6

* ŁUKASIEWICZ RESEARCH NETWORK – INSTITUTE OF NON-FERROUS METALS, LIGHT METALS DIVISION, 19 PIŁSUDSKIEGO STR., 32-050 SKAWINA, POLAND
** AGH UNIVERSITY OF SCIENCE AND TECHNOLOGY, FACULTY OF PHYSICS AND APPLIED COMPUTER SCIENCE, AL. MICKIEWICZA 30, 30-059 KRAKÓW, POLAND
[#] Corresponding author: sboczkal@imn.skawina.pl

solution [11]. Similar in vitro studies of the MgY2Zn1Ca0.22 alloy conducted in αMEM showed the initial pH value of 7.5 and after 100 hours the final pH value of 8.5 [12]. Alloys from the Mg-Li system showed the initial pH value of 8.0 and after 144 hours the final value of 9.3 [13]

In addition to properly selected alloying elements, the strength of the material also depends on the size of grains. Based on the results of studies it has been shown that grain refinement obtained as a result of severe plastic deformation (SPD) leads to an improvement in both mechanical and corrosive properties [14-20].

S.V. Dobatkin et al. described an example of the studies, in which the structure, strength and corrosion properties obtained as a result of rotary forging (RS), multiaxial deformation (MAD) and equal channel angular extrusion (ECAE) [20] were compared. It has been found that large plastic deformation of WE43 alloy in all three deformation schemes leads to a similar ultrafine-grained structure (UFG) characterized by the grain size of 0.5-1.0 μm and the presence of 0.3 μm Mg12Nd phase particles [20]. The UFG structure is reflected in the high level of mechanical properties of the WE43 alloy. Deformation by the ECAE and MAD methods increases the strength to 300 MPa as compared to 220 MPa in the initial state. There is also an increase in elongation to the level of 12-17%. In the case of the RS method, the tensile strength increases to 415 MPa, but at the expense of elongation which amounts to 7%. The assessment of corrosive properties has shown that the use of SPD methods does not weaken the resistance to electrochemical corrosion. The grain refinement by SPD methods largely improves the biocompatibility of the WE43 alloy [20].

Immersion tests in PBS carried out for 96 hours were made for samples produced by conventional extrusion and ECAE deformation method [14]. On the images of samples after corrosion tests, a clear difference in biodegradation between pure Mg and ZK60 alloy was observed. According to the authors, the influence of the phases occurring in the ZK60 alloy on the faster degradation process of this alloy was evident. Moreover, it has been found that the use of the ECAE method causes the inhibition of corrosion processes [14].

In recent years, the process of metal forming by ECAE has been extensively studied for Mg alloys. However, these studies generally included the assessment of mechanical properties and texture [22-28]. So far, only a few works on Mg alloys for biomedical applications deformed by the ECAE method have been published [29-32]. With the literature data so scarce, an attempt was made to study biomaterials in the form of MgLi alloys with the addition of Ca and Zn deformed by conventional extrusion and ECAE. The purpose of the work was to determine the effect of plastic forming processes on the dissolution rate of biocompatible Mg alloys. Additionally, the scope of work included issues related mainly to the possibility of controlling the structure of biocompatible alloys. The methods of plastic processing and their impact on grain refinement and strengthening were compared. The influence of structural constituents on the dissolution rate of alloys was analysed.

Methodology

The tests were carried out on two Mg-Li alloys with the addition of Ca and Zn in as-cast condition (Table 1). Casting into steel dies with a diameter of ø 40 mm and a length of 160 mm took place under a protective atmosphere of argon at >700°C.

TABLE 1

Chemical composition of castings [wt%]

Alloy	Li	Ca	Zn
MgLi1Zn1Ca0.2	0.68	0.23	0.81
MgLi1Zn1Ca1	0.68	0.92	0.82

The ingots of ø 38 mm and 50 mm length cast from MgLiCaZn alloys were subjected to indirect pressing at 350°C on a 100-ton vertical hydraulic press. For the ECAE process, samples of 10×10 mm and 50 mm length were prepared from extruded rods. The samples were deformed up to 3 passes in a 130° die at 350°C, rotating the sample after each pass in the Bc system.

The structure and grain size of the alloys after casting were examined on metallographic samples using an Inspect F50 scanning electron microscope with EDS detector and EBSD camera. The samples were taken from longitudinal sections and prepared by grinding and polishing on abrasive papers and polishing cloth with the following etching using a RES101 ion beam etching system. The EBSD analysis was made on a cross-sectional area of 400×400 μm with a step of 0.4 μm for samples after the extrusion process and on a cross-sectional area of 200×200 μm with a step of 0.3 μm for samples after the ECAE process. The analysis in the TSL OIM analysis software was made for grains with a 15° tolerance angle. Hardness was measured by Brinell method on a Duramin 2500.

The corrosion process was tested by immersion test in Ringer's solution with an osmolarity of 309 mOsmol/l, pH 5.0-7.5 and at 37°C on samples with a total surface area of about 280 mm^2. Corrosion was determined after 24, 48, 72 and 96 hours. The corrosion products were removed in accordance with ISO 8407 in a solution of $Cr0_3 + AgNO_3 + Ba(NO_3)_2$. The weight loss was determined based on weight measurements.

Macrostructure was examined on two samples of the MgLi1Ca0,2Zn1 alloy after 24 and 96 hours using a stereoscopic microscope as well as a Nanotom S nanotomograph from General Electric. The tomography image was recorded using a Hamamatsu detector (HAM C 7942CA-02) with a resolution of 12 bits and a matrix of 2300×2300 pixels.

Results and discussion

Structure and properties

Castings made from the MgLi1Ca0,2Zn1 and MgLi1 Ca1Zn1 alloys differed only slightly in the calcium content (0.8 wt%). However, even these differences in Ca content have translated into differences in the quantitative fraction of phases obtained, examined by the scanning microscopy (Fig. 1). In the MgLi1Ca0,2Zn1 alloy, small amounts of fine Mg_2Ca phases were observed in grain boundaries (Fig. 1a). In the structure of the MgLi1Ca1Zn1 alloy, the Mg_2Ca phase was also identified despite the fact that the point analysis of the chemical composition showed the presence of Zn [13]. The quantitative fraction of the Mg_2Ca phase in the MgLi1Ca1Zn1 alloy was higher than in the MgLi1Ca0,2Zn1 alloy and formed a network of precipitates within grains (Fig. 1b). The average grain size measured by the secant method showed a similar value of 120 μm for the MgLi1Ca0,2Zn1 alloy and 110 μm for the MgLi1Ca1Zn1 alloy.

The process of indirect extrusion of MgLiCaZn alloys was carried out at a relatively high temperature of 350°C. Attempts to use lower temperatures ended in failure due to the lack of possibility to control the deformation of materials tested.

The structure after the extrusion process observed by scanning microscopy has changed. The Mg_2Ca phases shown in Figures 2a and 2b were distributed along the extrusion direction. In the MgLi1Ca1Zn1 alloy, the finely fragmented phases were arranged along the grain boundaries more densely than in the MgLi1Ca02Zn1 alloy. A similar phase distribution in the tested alloys was observed after all 3 passes of the ECAE deformation process.

After extrusion of the rods, on SEM orientation maps, the distributions were examined on longitudinal sections (Figs. 3a and 4a). On the map made for the MgLi1Ca02Zn alloy, equiaxed grains were observed in which one or two of the polygonal boundaries were elongated in the direction of the deformation band. The image of the orientation distribution in the MgLi1Ca1Zn1 sample was different, and this was mainly due to the fact that the structure contained both large and small grains. For both tested alloys, the average grain size was about 10 mm, which means that it was by over 100 mm smaller than the grain size in as-cast state. In both samples after the extrusion process, twins were present inside the grains. The sample with 1% Ca content contained partially overgrown and fragmented twins. Both the size distribution of grains and the growth of twin boundaries evidenced the occurrence of dynamic renewal processes associated probably with a higher degree of strengthening obtained in the alloy with 1% Ca, and thus with a higher temperature of the extrusion process induced during friction.

a)
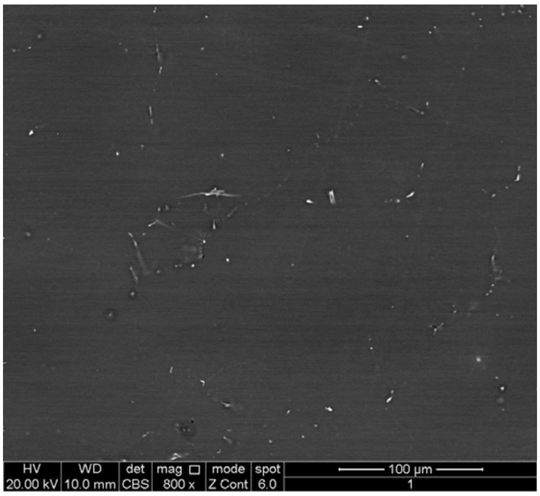

b)
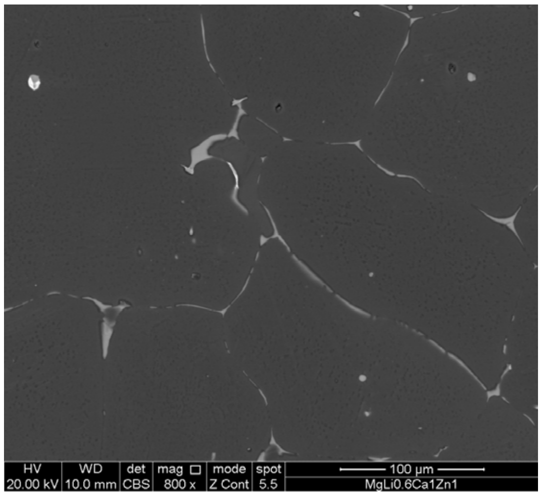

Fig. 1. The structure of alloys: a) MgLi1Ca02Zn1 and b) MgLi1Ca1Zn1 after casting

a)
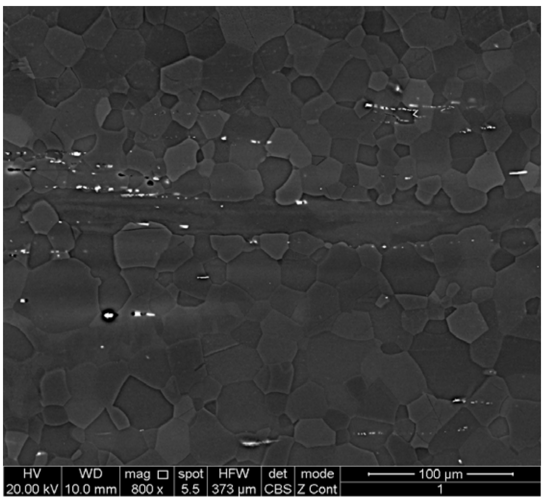

b)
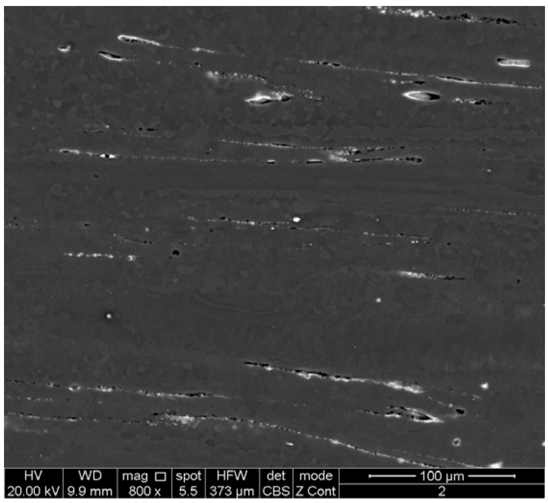

Fig. 2. The structure of alloys: a) MgLi1Ca02Zn1 and b) MgLi1Ca1Zn1 after extrusion

The samples after indirect extrusion were properly prepared and then deformed at a temperature of 350°C in the ECAE process up to the 3rd pass using a die angle of 130° (Figs. 3b-d and 4b-d). The structure of the samples was examined on a longitudinal section. On the orientation distribution maps, a low degree of grain refinement was observed compared to samples after extrusion. After the ECAE process, the smallest grain size of 2.8 mm was obtained for the MgLi1Ca0,2Zn1 alloy after the 3rd pass. The remaining samples after the ECAE process showed the grain size of approx. 7 mm. For both alloys tested, the grain size distribution after the 2nd pass was characterized by a wide range of values. Two types of grains were observed in the alloys, i.e. small grains of up to 35 μm in size, formed as a result of strong plastic deformation, and grains larger than 40 μm, which probably appeared due to the dynamic processes of structure recovery. Moreover, twins were visible inside the grains of the deformed samples. The highest fraction of twin boundaries was observed in the sample of MgLi1Ca0.2Zn alloy after the 3rd pass of the ECAE process.

Hardness (Table 2) was measured on samples after both the extrusion and ECAE process. Samples after the ECAP process showed an increase in strength as compared to the extruded samples. The hardness of the samples after the 1st pass was the highest and amounted to about 71HB for the MgLi1Ca0.2Zn1

TABLE 2

Hardness [HB]

Material	**As-cast**	**As-extruded**	**After the ECAE process**		
			I pass	**II pass**	**III pass**
MgLi1Ca0.2 Zn1	44,4±0,8	58,1±1,2	72,1±1,9	58,5±1,3	68,0±1,5
MgLi1Ca1 Zn1	46,5±1,1	57,2±1,1	70,9±1,4	76,8±1,2	69,7±1,8

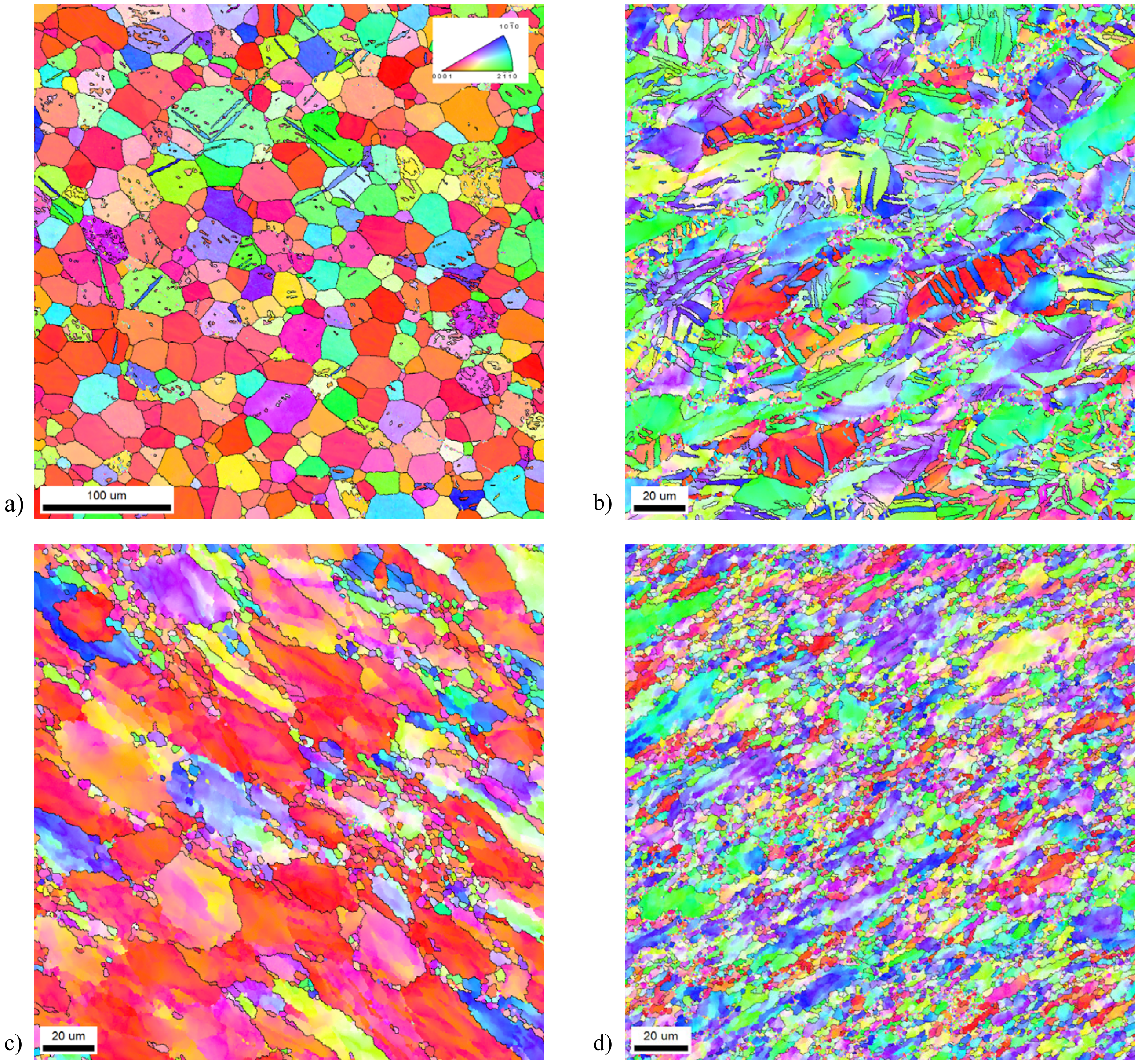

Fig. 3. Orientation distribution maps made for samples from the MgLi1Ca0,2Zn1 alloy cross-section after a) extrusion, b) 1st pass of ECAE, c) 2nd pass of ECAE and d) after the 3rd pass of ECAE

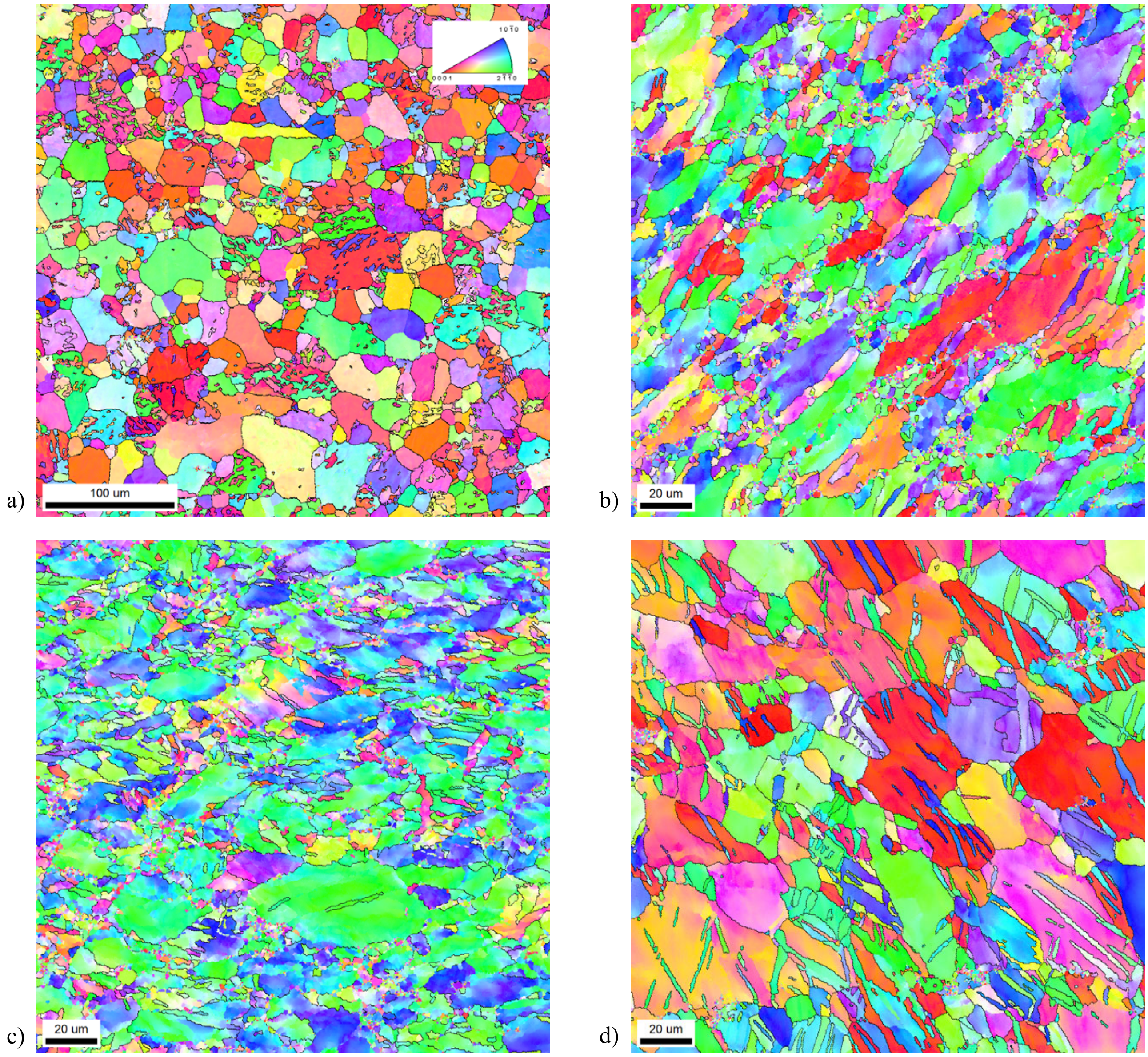

Fig. 4. Orientation distribution maps made for samples from the MgLi1Ca1Zn1 alloy cross-section after a) extrusion, b) 1st pass of ECAE, c) 2nd pass of ECAE and d) after the 3rd pass of ECAE

alloy. In subsequent passes, the strengthening effect decreased after the 2nd pass and increased after the 3rd pass to 68HB. In the case of the MgLi1Ca1Zn1 alloy, the highest level of strengthening was observed after the 2nd pass. For this sample, the hardness was 76.8 HB. After the 3rd pass of ECAE, the hardness decreased to 69HB.

A comparison of the EBSD results with hardness values shows that the higher fraction of recrystallized grains with equal and near orientation (111) in the alloy with 0.2% Ca content after the 2nd pass and in the alloy with 1% Ca content after the 3rd pass fully coincides with the strengthening effect. It is interesting to note that the alloy with a higher Ca content has reached the maximum level of strengthening after the 2nd pass, while the alloy with less Ca has reached this level immediately after the 1st pass. This is probably due to the state of material after the extrusion process, which in the MgLi1Ca1Zn1 alloy has initiated the mechanism of recrystallization.

The dissolution of Mg alloys

The biodegradation of magnesium alloys was tested in Ringer's solution at 37°C, taking out the samples after 24, 48, 72 and 96 hours and then performing measurements of the weight loss [%] for samples in different states. The differences in the dissolution rate observed in both tested casting alloys might be due to the differences in Ca content (Fig. 5). It has been demonstrated that Ca has a beneficial effect on the corrosion properties of magnesium alloys when it occurs in the alloy in an amount of less than 1% by weight, but the effect is negative when the level of 1% by weight is exceeded [34]. The analysis of weight loss graphs plotted as a function of time (Fig. 5) shows that plastic forming increases the degradation rate compared to the as-cast state of the alloys tested. The subsequent stages of MgLi1Ca0,2Zn1 alloy deformation contributed to a significant (>100 × greater) difference in the dissolution rate as compared

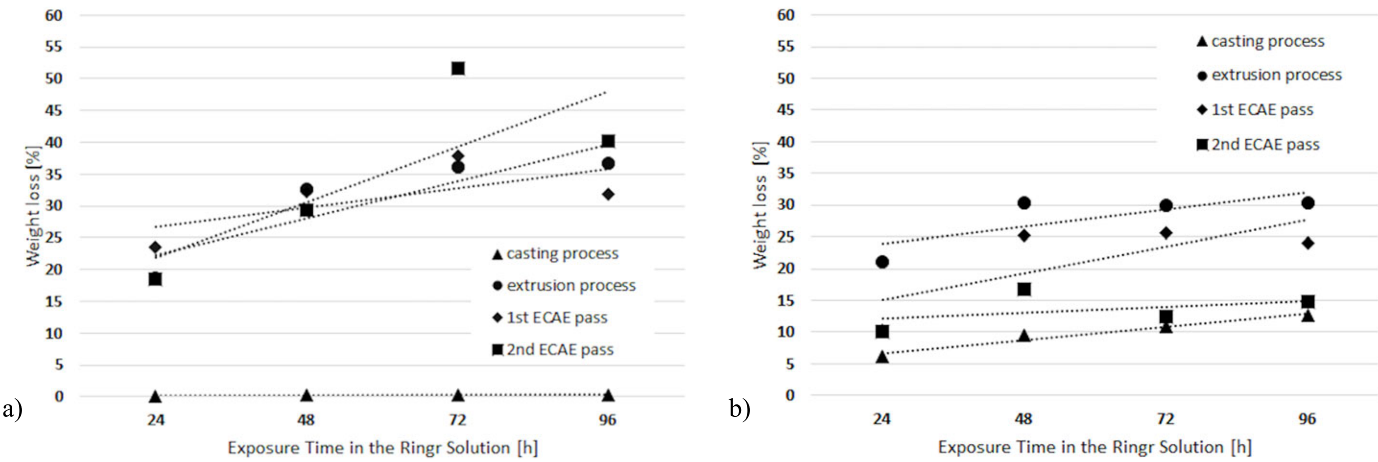

Fig. 5. Weight loss for: a) MgLi1Ca0,2Zn1 alloy samples and b) MgLi1Ca1Zn1 alloy samples

to the same alloy after casting (Fig. 4a). For this alloy, the dissolution rate was similar both after extrusion and deformation by ECAE. In the case of MgLi1Ca1Zn1 alloy, the highest weight loss of 30% after 96 h exposure was observed after extrusion (Fig. 5b). After the deformation by ECAE, the sample showed a lower dissolution rate, resulting after the 2^{nd} pass in the weight loss of 15%, i.e. two times lower than after extrusion. The decrease in the dissolution rate observed in the MgLi1Ca1Zn1 alloy after subsequent stages of the deformation process might be due to a stronger refinement of the structure in this alloy than in the MgLi1Ca0,2Zn1 alloy after the 2^{nd} pass, and thus to the increased number of grain boundaries. The increasing number of grain boundaries increases the number of crystal lattice defects. Studies described in [35] have shown that amorphous materials based on the Mg-Zn-Ca alloy dissolve more slowly than the same polycrystalline materials. Therefore it can be assumed that further ECAE process would lead to an even greater slowdown of the degradation process.

After immersion tests in Ringer's solution and removal of the reaction products, surface analysis of the samples was carried out.

Surface examinations after corrosion testing (Fig. 6) performed with a stereoscopic microscope showed the shape and location of pits. On the samples of MgLi1Ca0,2Zn1 alloy after extrusion, circle-shaped corrosion was observed (Fig. 6a), while samples after the 1^{st} and 2^{nd} pass of the ECAE process corroded along the corners (Fig. 6b,c). Characteristic circular grooves on the transverse surface might indicate the course of corrosion

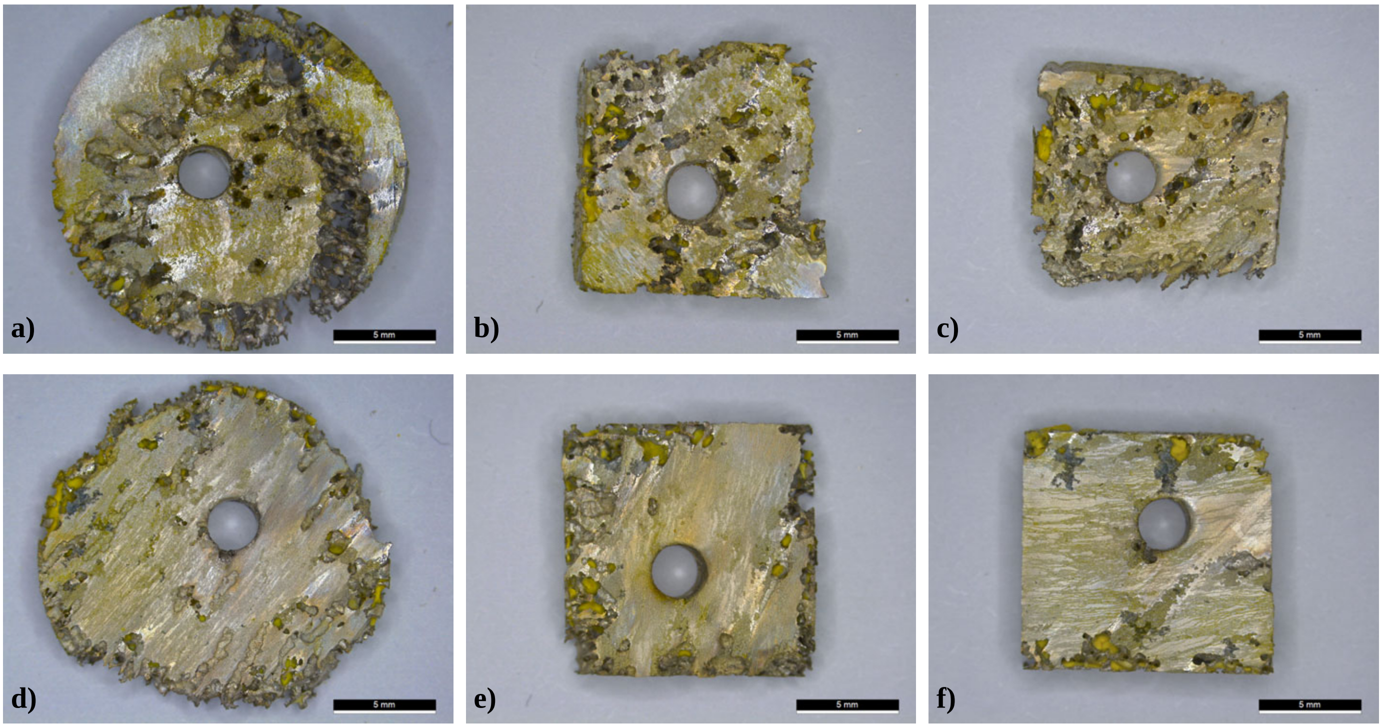

Fig. 6. Macrostructure of samples after 72 h exposure in Ringer's solution; MgLi1Ca0.2Zn1 alloy after: a) extrusion b) 1^{st} pass, c) 2^{nd} pass, and MgLi1Ca1Zn1 alloy after: d) extrusion, e) 1^{st} pass, f) 2^{nd} pass

along the metal flow lines originating from the "dead" zone in the die. In the MgLi1Ca1Zn1 alloy, pitting occurred in random distribution, mainly on the edges of the sample (Fig. 6d,e,f).

On the nanotomography images, pitting was observed in the cross-section and longitudinal section of the MgLi1Ca0,2Zn1 alloy sample after extrusion and 24 h and 96 h exposure in Ringer's solution (Fig. 7). After 24 h exposure, the longitudinal section showed a small depth of pitting in comparison to the sample after 96 h exposure. The sample extruded after 96 h exposure in the reagent showed pitting extending through the entire thickness of the sample. On both samples taken from the cross-section, pits arranged in the shape of a circle were visible.

SEM images allow determining the sequence of corrosion process (Fig. 8). The process of corrosion probably begins on the sample surface and largely depends on its development and roughness. The next phase of degradation occurs within particles and grain boundaries. The fastest to corrode are the boundaries with the highest energy [33] and the consequence is the formation of cavities of the grain size or larger. In the final stage, pits that often penetrate through the 2 mm thick sample are formed.

Conclusions

1. The grain refinement in the MgLi1Ca0,2Zn1 and MgLi1 Ca1Zn1 alloys was obtained as a result of extrusion and deformation process by the ECAE method. The grain size decreased by about 100 mm compared to as-cast alloys. After the ECAE process, the smallest grain size of 2.8 mm was obtained in the MgLi1Ca0,2Zn1 alloy after the 3rd pass.
2. In both alloys, an increase in hardness was observed after the extrusion process and after the deformation by ECAE, resulting in the latter case in a hardness of approximately 72HB after the 1st pass, which was higher than 58HB obtained after the extrusion process and 45HB after the casting process. The highest hardness was received for the MgLi1Ca1Zn1 alloy after the 2nd pass of the ECAE process.
3. Biodegradation tests carried out on alloys after the deformation process showed a much higher dissolution rate than the rate obtained in samples after the casting process. Weight

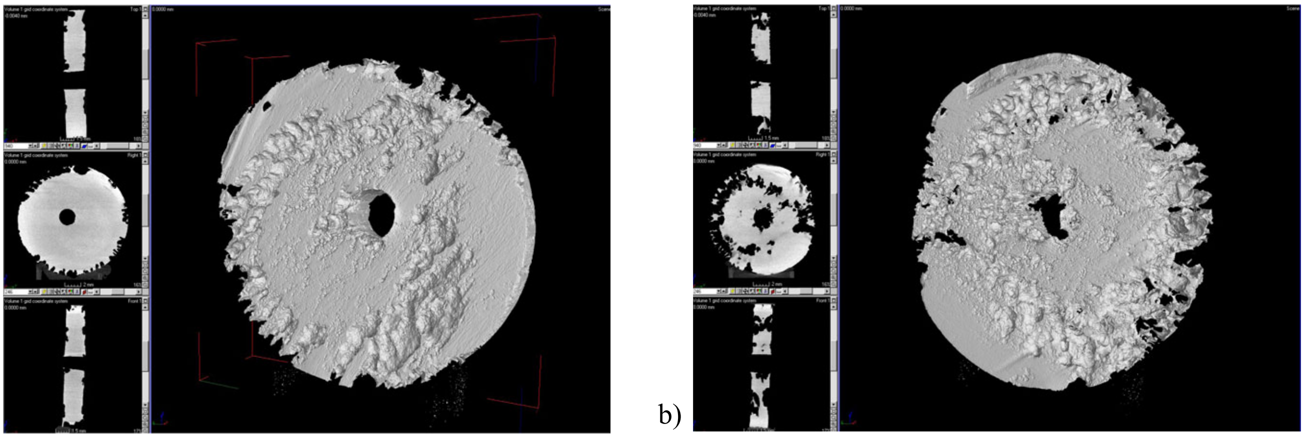
a) b)

Fig. 7. 3D nanotomography images of the cross-section and longitudinal section of the MgLi1Ca0,2Zn1 alloy sample after: a) 24 h and b) 96 h exposure in Ringer's solution

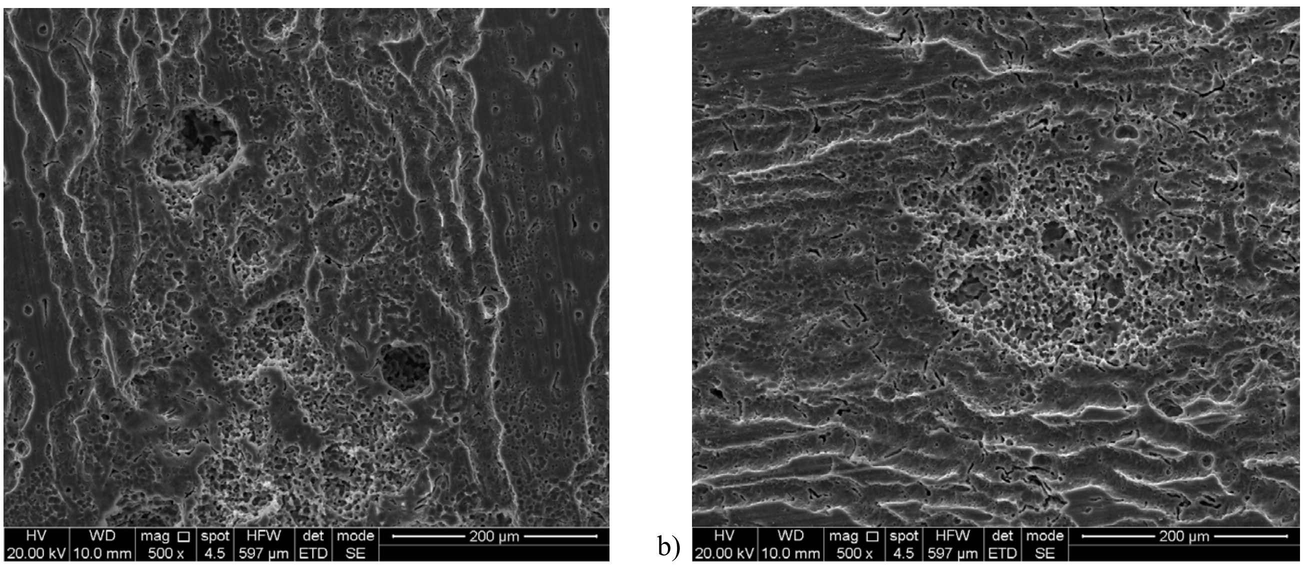

a) b)

Fig. 8. Examples of the SEM structure images obtained for alloys: a) MgLi1Ca0.2Zn1 and b) MgLi1Ca1Zn1 after 24 h exposure in Ringer's solution

loss after the deformation process ranged from 20 to 35%, while for both tested alloys after the casting process it did not exceed 7%.

4. In the case of the MgLi1Ca1Zn1 alloy, the increase in deformation and subsequent passes of the ECAE process reduced the dissolution rate, resulting in a lower weight loss after the 2nd pass of ECAE as compared to the samples extruded and samples after the 1st pass of ECAE.
5. Examinations carried out by stereoscopic microscopy, 3D nanotomography and SEM have revealed that degradation may occur not only on the surfaces and boundaries of phases and grains but also on the material flow lines originating from the "dead" zone in the die.

Acknowledgments

The authors gratefully acknowledge the financial support from the project no. 3787/E-138/S/2017 financed by the Ministry of Science and Higher Education.

REFERENCES

[1] D.T. Chou, D. Hong, J. Saha, J. Ferrero, B. Lee, Z. Tan, Z. Dong, P.N. Kumta, Acta Biomater. **9** (10), 8518-8533 (2013).
[2] X.N. Gu, Y.F. Zheng, Front Mater. Sci. China **4**, 2, 111-115 (2010).
[3] X.N. Gu, S.S. Li, X.M. Li, Y.B Fan, Front Mater. Sci. **8**, 3, 200-218 (2014).
[4] Y. Wan, G. Xiong, H. Luo,F. He, Y. Huang, X. Zhou, Mater. and Design **29**, 2034-2037, (2008).
[5] Z. Li, X. Gu, S. Lou, Y. Zheng, Biomat. **29**, 1329-1344, (2008).
[6] S. Boczkal, M. Lech-Grega, J. Żelechowski, Sol. St. Phen. **231**, 73-79, (2015).
[7] R. Zeng, W. Qi, F. Zhang, H Cui, Y Zheng, Prog. Nat. Sci.-Mater. **24**, 492-499, (2014).
[8] J. M. Rosalie, H. Somekawa, A Singh, T. Mukai, Mag. Tech. 323-328 (2013).
[9] L. Bao, Q. Le, Z. Zhang, J. Cui, Q. Li, J. Mag. and Alloys **1**, 2, 139-144 (2013).
[10] Y. Zheng, Magnesium Alloys as Degradable Biomaterials 2015, CRC.
[11] Q. Peng, Y. Huang, L. Zhou, N. Hort, K.U. Kainer, Biomat. **31**, 3, 398-403, (2010).
[12] A.C. Hänzi, I. Gerber, M. Schinhammer, J.F. Löffler, P.J. Uggowitzer, Act. Biomat. **6**, 1824-1833 (2010).
[13] S. Boczkal, M. Karaś, A. Osyczka, M. Lech-Grega, Mag. Tech. 399-404 (2018).
[14] E. Mostaed, M. Vedani, M. Hashempour, M. Bestetti, Biomatter. **4**, 1 (2014).
[15] D. Orlov, K.D. Ralston, N. Birbilis, Y. Estrin, Acta Mater. **59**, 6176-86 (2011).
[16] N.N. Aung, W. Zhou, Corros. Sci. **52,** 589-94 (2010).
[17] R.Z. Valiev, T.G. Langdon, Prog. Mater. Sci. **51**, 881-981 (2006).
[18] A. Yamashita, Z. Horita, T.G. Langdon, Mater. Sci. Eng. A **300**, 142-7 (2001).
[19] M. Alvarez-Lopez, M.D. Pereda, J.A. del Valle, M. Fernandez-Lorenzo, M.C. Garcia-Alonso, O.A. Ruano, M.L. Escudero, Acta Biomater. **6**, 1763-71 (2010).
[20] S. V. Dobatkin, et al, IOP Conf. Ser.: Mater. Sci. Eng. **194**, 012004 (2017).
[21] Q. Ge, D. Dellasega, A.G. Demir, M. Vedani, Acta Biomater. **9**, 8604-10 (2013)
[22] J. Li, W. Xu, X. Wu, H. Ding, K. Xia, Mater. Sci. Eng. A **528**, 5993-8 (2011)
[23] L.B. Tong, M.Y. Zheng, X.S. Hu, K. Wu, S.W. Xu, S. Kamado, Y. Kojima, Mater. Sci. Eng. A **527**, 16-17, 4250-4256 (2010)
[24] R. Ding, C. Chung, Y. Chiu, P. Lyon, Mater. Sci. Eng. A **527**, 3777-84 (2010).
[25] S. Li, Acta Mater. **56**, 1031-43 (2008).
[26] H.K. Lin, J.C. Huang, T.G. Langdon, Mater. Sci. Eng. A **402**, 250-7 (2005).
[27] S. Seipp,M.F.-X. Wagner, K. Hockauf, I. Schneider, L.W. Meyer, M. Hockauf, Int. J. Plast. **35**, 155-66 (2012)
[28] R. Waksman, R. Pakala, P.K. Kuchulakanti, R. Baffour, D. Hellinga, R. Seabron, F.O. Tio, E. Wittchow, S. Hartwig, C. Harder et al., Cath. Cardio Interv. **68**, 607-17 (2006).
[29] R. Erbel, C. Di Mario, J. Bartunek, J. Bonnier, B. de Bruyne, F.R. Eberli, P. Erne, M. Haude, B. Heublein, M. Horrigan et al., PROGRESS-AMS Lancet **369**, 1869-75 (2007).
[30] J. Vormann, Mol. Aspects Med. **24**, 27-37 (2003).
[31] G. Song, A. Atrens. Adv. Eng. Mater. **5**, 837-58 (2003).
[32] G. Song, Corros. Sci. **49**, 1696-701 (2007).
[33] K. Przybyłowicz, I. Suliga, Solid. Met. and All. **28**, 180-191 (1996).
[34] X. Gu, Y. Zheng, S. Zhong, T. Xi, J. Wang, W. Wang, Biomat. **31**, 1093-1103 (2010).
[35] R. Nowosielski, K. Cesarz, R. Babilas, Jour. of Achiev. in Mater. and Manuf. Engin. V **58**, 1, 7-15 (2013).